

# Empirical Attenuation of Ground-Motion Spectral Amplitudes in Southeastern Canada and the Northeastern United States

by Gail M. Atkinson

**Abstract** A database of 1700 digital seismograms from 186 earthquakes of magnitude  $m_N$  2.5–5.6 that occurred in southeastern Canada and the northeastern United States from 1990 to 2003 was compiled. Maximum-likelihood regression analysis of the database was performed to determine a model for the attenuation of Fourier spectral amplitudes for the shear window, for the vertical and horizontal component of motion, for frequencies from 0.2 to 20 Hz. Fourier amplitudes follow a hinged trilinear attenuation model. Fourier spectral amplitudes decay as  $R^{-1.3}$  (where  $R$  is hypocentral distance) within 70 km of the source. There is a transition zone from 70 to 140 km as the direct waves are joined by strong postcritical reflections, where the attenuation is described as  $R^{+0.2}$ ; spectral amplitudes actually increase with distance in this range for low frequencies. Beyond 140 km, the attenuation is well described by  $R^{-0.5}$ , corresponding to geometric spreading in two dimensions. The associated model for the regional quality factor for frequencies greater than 1 Hz can be expressed as  $Q = 893f^{0.32}$ .  $Q$  can be better modeled over a wider frequency range (0.2–20 Hz) by a polynomial expression:  $\log Q = 3.052 - 0.393 \log f + 0.945 (\log f)^2 - 0.327 (\log f)^3$ . The polynomial expression accommodates the observation that  $Q$  values are at a minimum (about 1000) near 1 Hz and rise at both lower and higher frequencies. Correction factors for the spectral amplitude model that describe the effects of focal depth on the amplitudes and their attenuation are developed using the subset of events with known focal depth. The attenuation model is similar to that determined from an earlier study with more limited data (Atkinson and Mereu, 1992), but the enlarged database indicates more rapid near-source amplitude decay and higher  $Q$ .

The attenuation model is used to play back attenuation effects to determine the apparent source spectrum for each earthquake in the database and hence determine moment magnitude ( $M$ ) and Brune stress drop. The events have moment magnitude in the range from 2.5 to 5. Stress drop increases with moment magnitude for events of  $M < 4.3$ , then appears to attain a relatively constant level in the range from 100 to 200 bars for the larger events, as previously noted in Atkinson (1993b).

The results of this study provide a useful framework for improving regional ground-motion relations in eastern North America. They further our understanding of attenuation in the region through analysis of an enlarged ground-motion database. In particular, the inclusion of the three-component broadband data gathered over the last decade allows extension of attenuation models to both horizontal and vertical components over a broad frequency range (0.2–20 Hz).

## Introduction

The attenuation of ground-motion amplitudes in the frequency domain is an important problem in engineering seismology. It is of particular practical interest in regions such as eastern North America (ENA), where seismographic data of moderate events are relatively abundant but strong-motion data are lacking. In such cases, an empirical attenuation

model determined from moderate events provides critical input to models of ground-motion generation and propagation from larger events. These ground-motion relations are a key input to seismic hazard analysis for engineered structures. Commonly used engineering ground-motion relations for ENA that rely on an empirical model of attenuation in-

clude the stochastic-model relations of Atkinson and Boore (1995), Toro *et al.* (1997), and Frankel *et al.* (1999) and the hybrid-empirical model of Campbell (2003). All of these relations use as input the spectral attenuation model for ENA determined by Atkinson and Mereu (1992). The Atkinson and Mereu attenuation model was derived from analysis of approximately 1000 digital short-period vertical-component seismograms recorded from 1980 to 1990 on the Eastern Canada Telemetered Network (ECTN). In recent years, the ENA seismographic database has grown significantly, as data continue to accumulate. Furthermore, most of the short-period vertical-component instruments in southeastern Canada have been replaced with the broadband three-component instruments of the Canadian National Seismographic System (CNSN) (operated by the Geological Survey of Canada). (Note: Regrettably, the upgrading of instruments in the northeastern United States has not kept pace due to political delays in the implementation of the Advanced National Seismic System.) It is therefore timely to revisit the attenuation model of Atkinson and Mereu (1992), refining it to include new data gathered since 1990. The attenuation model can also be improved by extending it over a broader bandwidth. The ECTN data of 1990 produced an attenuation model that was valid from 1 to 10 Hz, whereas the the broadband data can be used to develop an attenuation model from approximately 0.2 to 20 Hz. Furthermore, since CNSN and U.S. National Seismic Network (USNSN) stations are three component, the new model can explicitly address horizontal-component ground motions, which are of most engineering interest.

In this study, I perform regression analyses to determine an attenuation model for Fourier spectra of earthquakes in southeastern Canada and the northeastern United States, using digital seismographic data gathered through 2002. The data sources include the older ECTN database analyzed in Atkinson and Mereu (1992) plus broadband three-component data recorded primarily on the CNSN from 1997 through 2002, for earthquakes of Nuttli magnitude ( $m_N$ ) 2.5–5.6. The new data allow attenuation and source issues to be addressed over a much broader bandwidth than was possible in the previous data analyses of Atkinson and Mereu (1992) and widen the scope to three components of motion.

The regression analysis will be used to determine the shape and level of attenuation of Fourier spectral amplitudes for the *S* window as a function of frequency; the *S* window is selected to include the strongest shaking, as this is the portion of the signal of most engineering significance. In previous studies (Atkinson and Mereu, 1992; Atkinson and Boore, 1995), it has been determined that the attenuation can be described by a hinged-trilinear form, in which the slope of the attenuation relation is different in three distance ranges (<70, 70–130, and >130 km). This is explained by the transition in wave types dominating the signal that makes up the *S* window. At close distances the signal is composed of direct waves whose amplitudes decay due to geometrical spreading in a whole space. Beyond 70 km, the presence of

strong postcritical reflections from the Moho discontinuity cause flattening of the attenuation curve, leading to little apparent attenuation between approximately 70 and 130 km (Burger *et al.*, 1987; Somerville and Yoshimura, 1990; Atkinson and Mereu, 1992). At large distances (>130 km) the signal contains multiply reflected and refracted waves traveling in the crustal wave guide (Herrmann and Kijko, 1983; Kennett, 1986; Shin and Herrmann, 1987; Ou and Herrman, 1990; Bowman and Kennett, 1991).

The regression analysis of this study will revisit both the form and the hinge points of this attenuation function, as well as determining a new *Q* (quality factor) model to describe the associated anelastic attenuation. Source parameters for moderate earthquakes will also be determined by the regression analysis. The attenuation and source information is important for modeling ground motions from future large earthquakes, particularly at intermediate frequencies, which have not been well represented in previous databases.

The predictive magnitude variable for the regressions is  $m_1$ , determined from the 1-Hz spectral amplitudes as defined in Chen and Atkinson (2002):

$$m_1 = 4.4665 + 0.7817 \log (A_1)_{10} + 0.1399[\log (A_1)_{10}]^2 + 0.0351[\log (A_1)_{10}]^3, \quad (1)$$

where  $(A_1)_{10}$  is the 1-Hz spectral acceleration in centimeters per second at a reference distance of 10 km. To determine  $(A_1)_{10}$ , the attenuation curve determined by the regression model (equation 2) is assumed (with the set model parameters of  $b_1$ ,  $b_2$ ,  $b_3$ ,  $R_{11}$ , and  $R_{12}$  for that regression trial, as described later), with the initial estimate of anelastic attenuation given by  $c_4$  (1 Hz) = 0.00035. For each event,  $m_1$  is determined as the average value over all stations in the database that recorded the earthquake. (Note: The regression is iterated if the final estimate of  $c_4$  at 1 Hz differs significantly from the initial estimate. Thus I ensure that the determined  $m_1$  values are consistent with the final regression model.) Figure 1 compares the determined values of  $m_1$  to the catalog values of  $m_N$  for all earthquakes in the spectral database. The advantages of using  $m_1$  as the predictive magnitude variable are that (1)  $m_1$  characterizes the strength of the earthquake signal in a clearly defined frequency range and (2)  $m_1$  is nearly equal to moment magnitude for the moderate earthquakes of this study, as will be shown later.

### Database for Analysis

Figure 2 shows the locations of earthquakes and seismographic stations used in this study; different symbols are used to distinguish the new broadband CNSN/USNSN stations from the older short-period ECTN stations. The new data include several notable events, including three events of  $m_N > 5$  (1997 Cap Rouge, Quebec; 2000 Kipewa, Ontario; and 2002 Au Sable Forks, New York, earthquakes). All sta-

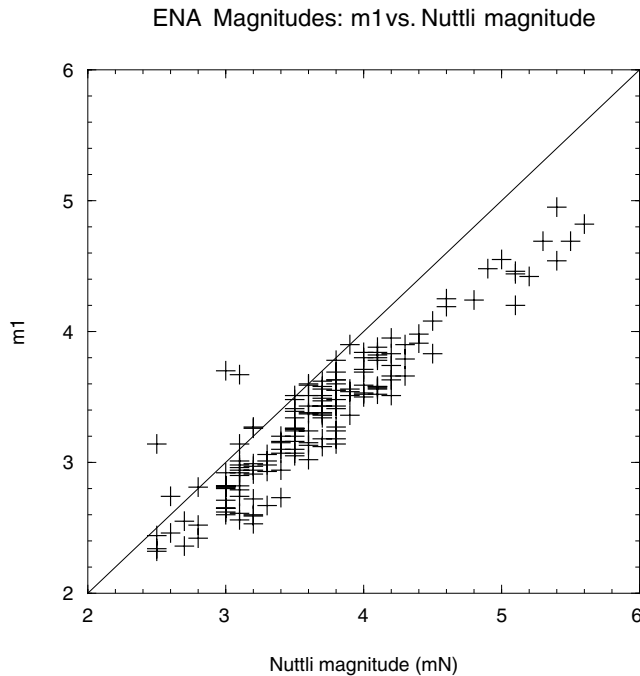


Figure 1. Relationship between the 1-Hz magnitude measure  $m_1$  and Nuttli magnitude  $m_N$  for the study earthquakes.

tions used in this study are sited on bedrock. Seismic refraction surveys at selected sites in southeastern Canada suggest that the average shear-wave velocity for a typical rock site is about 2.8 km/sec (Beresnev and Atkinson, 1997). Stations in the Charlevoix seismic zone may have somewhat lower shear velocities owing to the meteorite impact structure that has resulted in a highly fractured upper crust in that region.

The ECTN data to 1990 were previously processed and tabulated in Atkinson and Mereu (1992). Briefly, for each record the window of strongest shaking (shear window, including direct, reflected, and refracted phases) was selected, and a 5% taper was applied at each end of the window. The Fourier spectrum of acceleration was determined, correcting for instrument response. The spectra were smoothed and tabulated in increments of 0.1 log frequency units, for log frequencies of 0 to 1 (e.g., 1–10 Hz). Spectra for a pre-event noise window, normalized to the same duration as the signal window, were processed and tabulated in the same manner. Data were retained for further analysis only at frequencies for which the signal-to-noise ratio exceeds 2.

The broadband CNSN data for events from November 1997 through December 2002 (plus an event of  $m_N$  4.1 that occurred in June 2003) were compiled and processed in a similar manner to that used for the ECTN data. In the case of CNSN data, however, the spectra were smoothed and tabulated in 0.1 log frequency increments over log frequencies from  $-1$  to  $1.3$  (e.g., 0.1–20 Hz). The smoothing applied takes the geometric average of the spectral amplitudes in

each log frequency bin; thus the log spectral amplitude at log frequency = 1.0 is the average log amplitude for all spectral values with  $0.95 \leq \log \text{frequency} < 1.05$ , for example. Data were compiled for the shear window for the vertical component and two horizontal components at each CNSN station. A minimum signal-to-noise criterion of 2 was adopted.

Finally, the compiled spectral data were checked to eliminate data in magnitude–distance ranges affected by low-amplitude quantization noise problems. Amplitudes are not reliably recorded where the signal strength is not sufficiently strong relative to the minimum level that the instrument can detect (regardless of signal-to-noise ratio). This problem can be detected in the processed data by plotting amplitudes versus distance for all data within a limited magnitude range, then examining such plots for evidence of a floor in the recorded spectral amplitudes that may appear beyond certain distances. The low-amplitude floor problem is frequency dependent, affecting low frequencies more strongly than higher frequencies. Based on examination of amplitude plots, I retained CNSN data within the distance limits given in Table 1.

Figure 3 shows the magnitude–distance range for the compiled vertical-component data for  $f \geq 1$  Hz, distinguishing between ECTN and CNSN/USNSN data. Data at lower frequencies are available only for the CNSN/USNSN subset of the database (subject to the limits described earlier). Horizontal-component data are available for the CNSN/USNSN data and a limited subset of the ECTN data (as described by Atkinson [1993a]). It should be noted that a few records for larger events exist, notably the records from the 1988  $m_N$  6.5 Saguenay, Quebec, earthquake and distant records from two earthquakes of  $m_N$  5.7 and 6.1 in northern Quebec in 1989. These data are not included in the regression because the sampling of the magnitude space above magnitude  $m_N$  5.6 is too sparse and might bias the determination of the magnitude scaling of the spectral amplitude model. However, the attenuation model may still be used to estimate near-source amplitudes for these events if desired, by playing back the attenuation effects for each event.

### Regression Methodology and Form

Regression is performed by the maximum-likelihood method using the algorithm of Joyner and Boore (1993, 1994). Because of the wealth of vertical-component data, the regressions initially focus on the vertical component, then the horizontal component is addressed later in the article. I fit the observed Fourier amplitudes at each specific frequency to an equation of the general form

$$\log A_{ij} = c_1 + c_2 (M - 4) + c_3 (M - 4)^2 - b \log R - c_4 R, \quad (2)$$

where  $A$  is the observed spectral amplitude,  $R$  is hypocentral

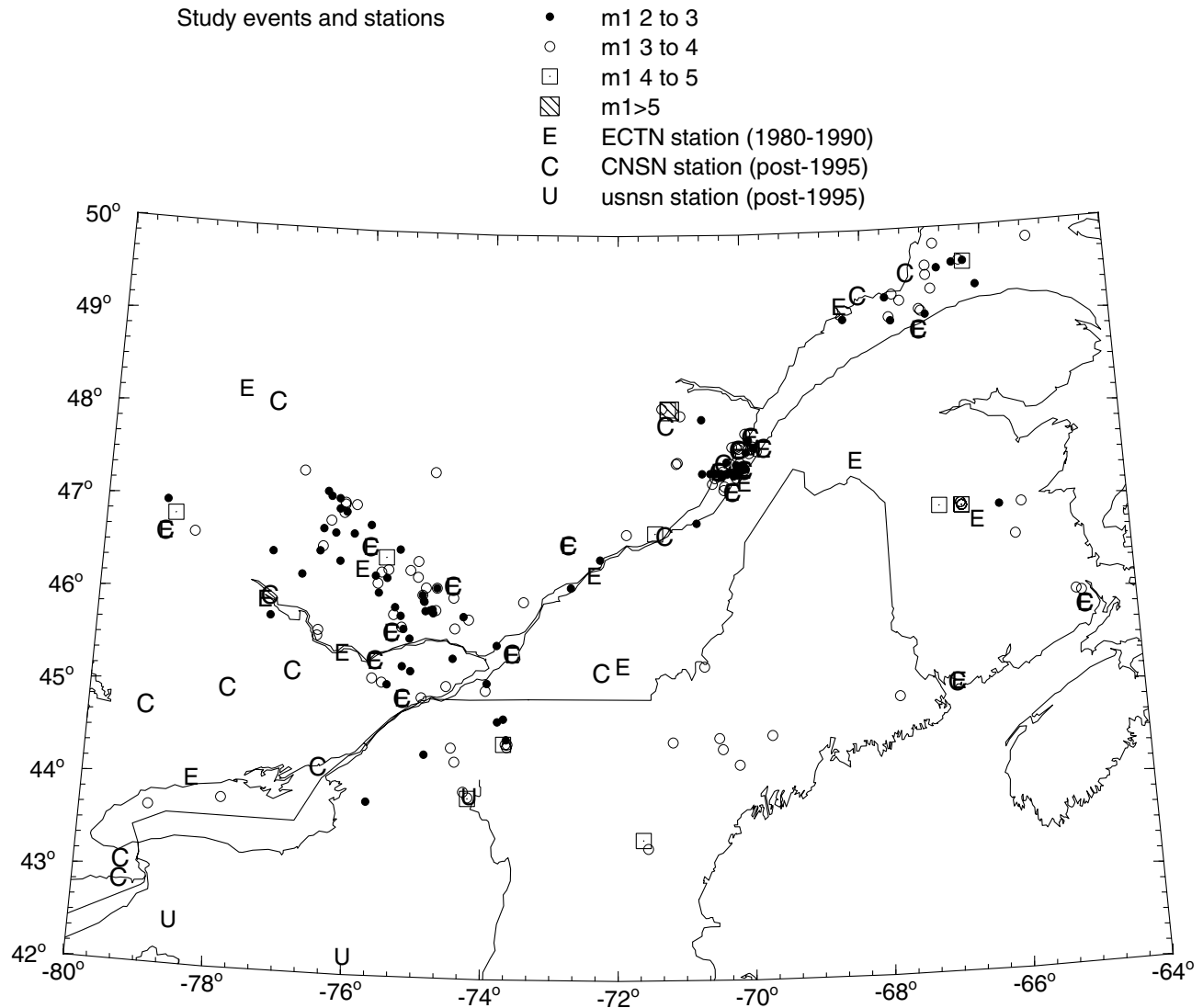


Figure 2. Locations of the study earthquakes and seismographic stations. Note that ECTN stations obtained vertical-component data over the 1- to 10-Hz frequency range for events up to 1990. Post-1995 data are from the three-component broadband stations of the CNSN and USNSN.

Table 1  
Distance Limits For Reliable Amplitudes

	$f < 1$ Hz (km)	$f \geq 1$ Hz (km)
$m_N < 3$	0	100
$3 \leq m_N < 3.5$	80	200
$3.5 \leq m_N < 4$	100	400
$4 \leq m_N < 4.5$	200	800
$m_N \geq 4.5$	800	2000

distance,  $b$  is the assumed (or determined) geometric spreading coefficient, and  $c_1$  through  $c_4$  are the coefficients to be determined.  $M$  is a magnitude measure. The most commonly available magnitude for the events from the earthquake catalogs is  $m_N$ . The optimal magnitude measure would be mo-

ment magnitude ( $M$ ), but this is available for only a few of the larger events. Moment magnitude can be determined for most of the events of this study, especially those for which broadband data are available, but only after detailed evaluation of the regression model and results. I therefore use the intermediate spectral magnitude measure  $m_1$ , as defined in Chen and Atkinson (2002), as the predictive magnitude variable. I choose  $m_1$  because it is simple to determine at the outset of the study and is a close approximation to  $M$  for events of  $M < 5$ , which dominate the database (shown later in Fig. 16). No site response term is included in equation (2) because all recordings are on hard-rock sites. The results are thus applicable to typical hard-rock site conditions in ENA. Variability in site response among the rock sites is evaluated later in the article based on analysis of regression residuals

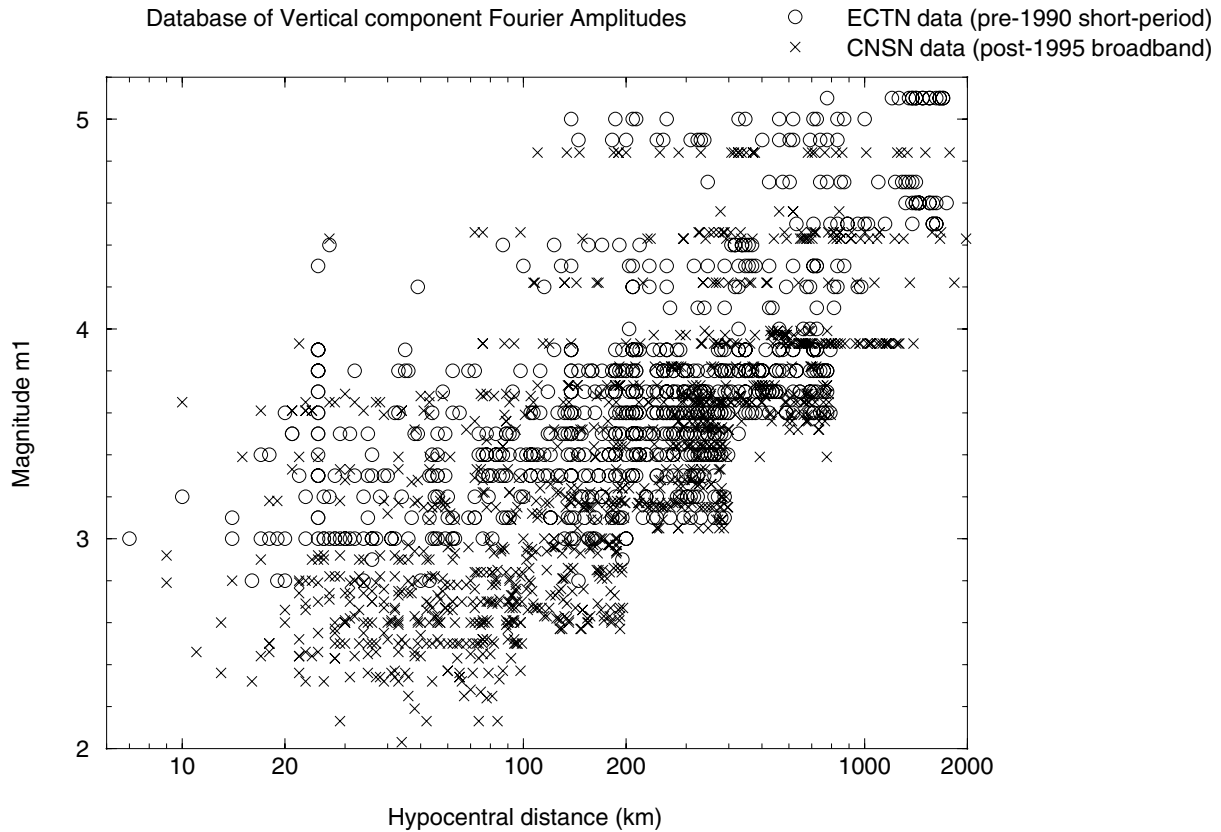


Figure 3. Distribution of the study ground-motion database (vertical component) in magnitude ( $m_1$ ) and hypocentral distance. Circles show ECTN data (vertical component, short period). X's show CNSN/USNSN data (three-component broadband).

on a site-by-site basis. The anelastic coefficient,  $c_4$ , is inversely related to the quality factor,  $Q$ :

$$Q = (\pi f) / [\ln(10) c_4 \beta], \quad (3)$$

where  $\beta$  is the shear-wave velocity (e.g., Atkinson and Mereu, 1992).

In applying the general form of equation (2), the coefficient  $b$  is allowed to take on different values in different distance ranges, to accommodate the geometric attenuation behavior of the shear window as different phases arrive. Within approximately 70 km of the earthquake source, the shear window is dominated by the direct  $S$ -wave arrival. Within the distance range from about 70 to 120 km, the direct  $S$  wave is joined by the first postcritical reflections from the Conrad and Moho discontinuities (Burger *et al.*, 1987). At distances beyond about 100–150 km, the signal is dominated by the  $Lg$  phase, consisting of multiply reflected and refracted shear waves (Herrmann and Kijko, 1983; Kennett, 1986; Shin and Herrmann, 1987; Ou and Herrmann, 1990; Bowman and Kennett, 1991). The attenuation behavior varies with distance according to these arrivals. Atkinson and Mereu (1992) and Atkinson and Boore (1995) used a hinged trilinear shape to model attenuation, where the co-

efficient  $b$  was given by  $b_1 = 1.0$  from the source to 70 km ( $=R_{11}$ ),  $b_2 = 0.0$  from 70 ( $=R_{11}$ ) to 130 km ( $=R_{12}$ ), then  $b_3 = 0.5$  beyond 130 km ( $=R_{12}$ ), corresponding to direct arrivals, strong reflections, and surface-wave spreading, respectively.

In this study, the attenuation model follows the hinged trilinear shape determined in Atkinson and Mereu (1992), but I redetermine the slopes ( $b_1$  and  $b_2$ ) and hinge points ( $R_{11}$  and  $R_{12}$ ) of the attenuation model. The attenuation beyond  $R_{12}$ , corresponding to surface-wave spreading of multiply reflected and refracted shear waves in the crustal wave guide, is well established from previous studies (Herrmann and Kijko, 1983; Kennett, 1986; Shin and Herrmann, 1987; Ou and Herrmann, 1990; Bowman and Kennett, 1991; Atkinson and Mereu, 1992) and is therefore fixed at  $b_3 = 0.5$ . The best-fit attenuation model is determined by repeating the regressions many times to search the parameter space defined by the selected transition distances ( $R_{11}$  and  $R_{12}$ ) and geometric coefficients ( $b_1$  and  $b_2$ ). All combinations of the following model parameters for the regression are evaluated:  $R_{11} = 50, 60, 70, \dots, 100$ ;  $R_{12} = 100, 110, 120, \dots, 200$ ;  $b_1 = 1.0, 1.1, 1.2, \dots, 1.6$ ;  $b_2 = -0.5, -0.4, -0.3, \dots, +0.5$ ; and  $b_3 = 0.5$ . Note that this parameter space covers the possibility of a hinged bilinear model (single transition distance) as well as the hinged trilinear model. The best-fit

attenuation model is that which produces the lowest average error (lowest residuals) over the frequency range from 1 to 10 Hz (for which the data are most abundant).

The best-fit shape for the attenuation model is obtained when  $b_1 = 1.3$ ,  $b_2 = -0.2$ ,  $b_3 = 0.5$ ,  $R_{t1} = 70$  km, and  $R_{t2} = 140$  km. This is similar to the result of Atkinson and Mereu (1992), but with steeper attenuation near the source and negative attenuation in the transition zone (low-frequency amplitudes actually increase slightly from 70 to 140 km). The finding that the attenuation within 70 km of the source is clearly steeper than  $R^{-1}$  is perhaps a surprising result of this study. Interestingly, J. Boatwright (personal comm., 2003) has reported a similar finding in regression of seismographic data from moderate events in California and argued that this effect is a consequence of directivity. Sonley (2004) has also reported near-source attenuation steeper than  $R^{-1}$  in the Charlevoix region; this finding was based on using the reverse two-station method of Chun *et al.* (1987) to eliminate source and site effects, isolating path effects only. Herrmann and Malagnini (2004) used synthetic seismograms generated for a number of crustal models, focal mechanisms, and depths to show that attenuation is expected to depart from  $R^{-1}$  for many cases, especially for typical thrust events in eastern North America. The attenuation shape is illustrated in Figure 4, which plots the spectral amplitudes for a subset of the data of  $m_1$  3.5–4.0, in comparison to the determined attenuation model.

It may not be clear from Figure 4, which shows only a subset of the data, that an attenuation slope steeper than 1.0 is really required for  $R \leq 70$  km, particularly given possible parameter trade-offs. Since this is an important new finding, I explore it in more detail to assess the confidence with which this conclusion can be drawn. The shape of the near-

source attenuation can be explored by using just earthquakes that were recorded within 70 km on at least three stations; there are 270 data points in this subset. I assume that the source spectra for each earthquake in this subset, at low to intermediate frequencies, can be estimated by correcting all observed spectra for geometric spreading by multiplying by  $R$  (thus I am not preconditioning the result in any way by assuming a steeper attenuation). At frequencies  $\leq 2$  Hz, anelastic attenuation effects for observations within 70 km are negligible ( $<10\%$ ). The source spectra for each earthquake is estimated by averaging (log average) the attenuation-corrected spectra over all stations that recorded the event (hence the requirement that each event be recorded at at least three stations). I then subtract the log source spectrum for the event from each of its observed log spectra, to obtain spectral amplitudes that have been normalized to a common source level (log amplitude = 0 at  $R = 1$  km). The normalized spectral amplitudes are thus defined as

$$\log An_{ij}(f) = \log A_{ij}(f) - (1/N) \sum_{i=1}^N [\log A_{ij}(f) + \log R_{ij}], \quad (4)$$

where  $An_{ij}$  is the normalized amplitude for earthquake  $i$  at station  $j$ ,  $A_{ij}$  is the observed amplitude of earthquake  $i$  at hypocentral distance  $R_{ij}$ , and the sum is over the  $N$  stations that recorded earthquake  $i$ . Figure 5 plots the log normalized spectral amplitudes at a frequency of 2 Hz, along with the mean and 90% confidence limits of these data grouped into distance bins that are 0.2 log units in width. It is clear on Figure 5 that the attenuation is significantly steeper than that defined by  $1/R$ . Regression of the normalized log amplitudes

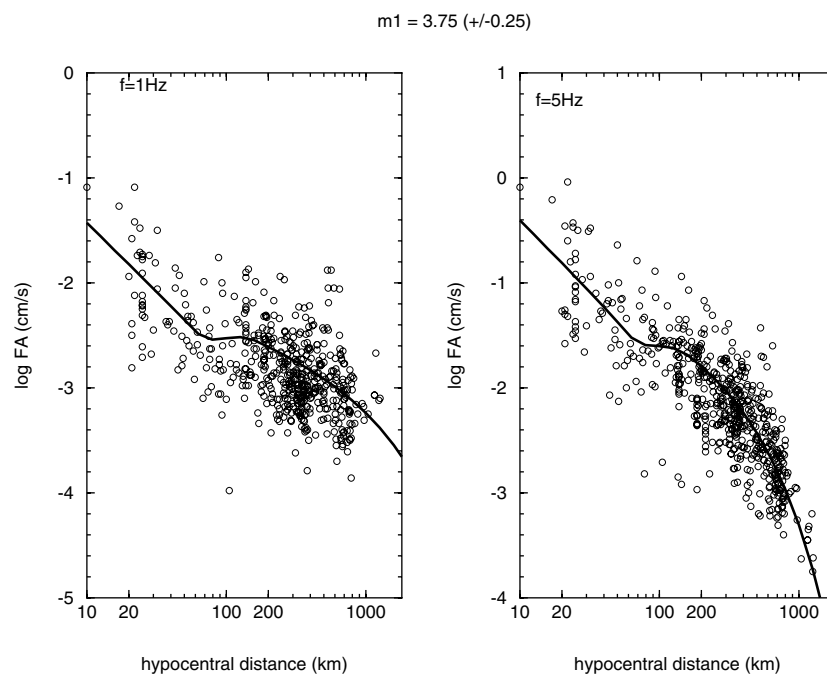


Figure 4. Vertical-component Fourier spectral amplitudes in the shear window for events of  $m_1$  3.5–4 (circles), at 1 and 5 Hz, compared to prediction equation developed from regression model (lines).

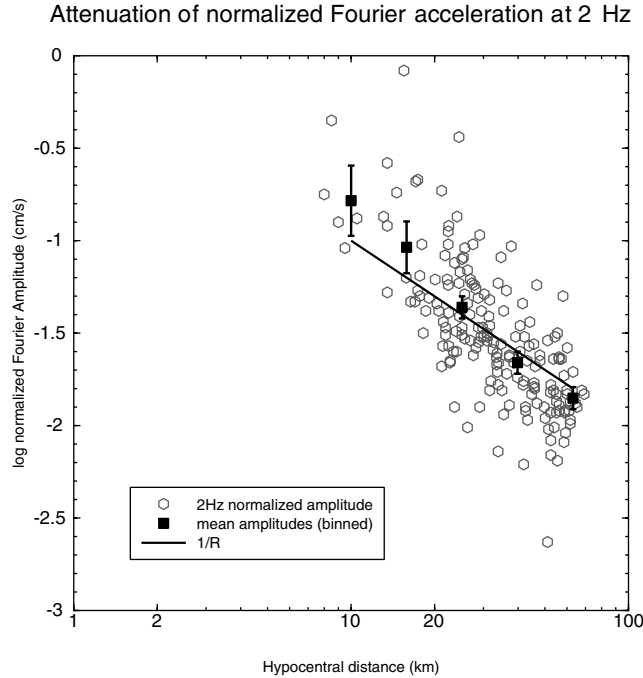


Figure 5. Attenuation of normalized 2-Hz Fourier spectral amplitudes, for all events having at least three observations within 70 km of the earthquake source. Normalization is done by subtracting an initial estimate of the earthquake's source amplitude from each observation.

of Figure 5 indicates a slope of 1.41, with 95% confidence limits of 0.19 on the slope coefficient. Thus we can be 95% confident that the true slope is steeper than 1.2.

## Results

### Vertical-Component Attenuation Model

Table 2 provides the regression coefficients for the fit of the vertical-component data set to the regression equation, which can be written as

$$\log A = c_1 + c_2 (m_1 - 4) + c_3 (m_1 - 4)^2 - 1.3 \log R - c_4 R \quad \text{for } R \leq 70 \text{ km}, \quad (5a)$$

$$\log A = c_1 + c_2 (m_1 - 4) + c_3 (m_1 - 4)^2 - 1.3 \log (70) + 0.2 \log (R/70) - c_4 R \quad \text{for } 70 < R \leq 140 \text{ km}, \quad (5b)$$

$$\log A = c_1 + c_2 (m_1 - 4) + c_3 (m_1 - 4)^2 - 1.3 \log (70) + 0.2 \log (140/70) - 0.5 \log (R/140) - c_4 R \quad \text{for } R > 140 \text{ km}. \quad (5c)$$

The standard errors of the regression coefficients are typically about 0.02 for  $c_1$ , 0.03 for  $c_2$ , 0.02 for  $c_3$ , and 0.00003 for  $c_4$ . Thus the coefficients  $c_1$ ,  $c_2$ , and  $c_4$  are well determined, while the  $c_3$  coefficient (the quadratic term in magnitude) is not significant at some frequencies.

The data variability, given by the standard deviation of residuals (sigma), is relatively large (factor of about 2 at most frequencies). This is not surprising, especially given the large magnitude and distance range of the data. The  $Q$  value implied by the  $c_4$  coefficient (equation 3) is also listed in Table 2. The  $Q$  values are systematically higher than those found by Atkinson and Boore (1995), which is explained by the differences in the associated geometric spreading coefficients. For frequencies above 1 Hz, the  $Q$  values can be fit by the commonly used exponential form as

$$Q = 893f^{0.32}. \quad (6)$$

As shown in Figure 6, a better fit is obtained, over all frequencies, by a third-degree polynomial:

$$\log Q = 3.052 - 0.393 \log f + 0.945 (\log f)^2 - 0.327 (\log f)^3. \quad (7)$$

The polynomial form accommodates the observation that  $Q$  values are at a minimum (1000) near 1 Hz and rise at both lower and higher frequencies. However, the cubic polynomial should not be extrapolated beyond 50 Hz, as equation (7) results in decreasing  $Q$  for  $f > 50$  Hz. Boore (2003) reported a similar U-shape for  $Q$ , based on a survey of Aki (1980) and Cormier (1982).

Figure 7 plots the residuals of the regression against distance, where the log residual is defined as the log of the observed spectral amplitude minus the log of the predicted spectral amplitude according to equation (5). There are no discernible trends in the residuals when plotted against distance. In Figure 8, I plot the residuals for data with known focal depths (at a frequency of 5 Hz) to determine if there is evidence for depth-dependent effects in the attenuation. There is a clear depth effect on attenuation that is apparent in this figure, with events deeper than 20 km showing low amplitudes near the source and large amplitudes at large distances, relative to the average attenuation model. Events shallower than 8 km show an opposing trend. This tendency is modeled by regressing the log residuals against the term  $[(h - 10) \log R]$ , where  $h$  is the focal depth in kilometers and  $R$  is hypocentral distance in kilometers. The term  $(h - 10)$  is used in the regression because 10 km is near the average focal depth of the data set. Table 3 provides the coefficients of this regression. The focal depth effects are most significant at frequencies of 5–10 Hz; they become insignificant for frequencies less than 1 Hz. These coefficients may be used to estimate correction factors for the ground-motion amplitudes given by equation (5), based on focal depth. The factors given by Table 3 may be added to the predictions of equation (5) (or subtracted from the observations) to obtain

Table 2  
Coefficients of Regression for Vertical-Component Fourier Amplitudes (equation 5)

Frequency	$c_1$	$c_2$	$c_3$	$c_4$	$\sigma$	$n_{obs}$	$Q$
0.20	-0.305	0.895	0.2294	0.00000	0.46	241	
0.25	-0.324	0.961	0.2665	0.00000	0.39	253	
0.32	-0.296	1.066	0.2489	-0.00003	0.38	291	3388
0.40	-0.278	1.435	0.4174	-0.00006	0.32	358	2424
0.50	-0.193	1.614	0.3903	-0.00009	0.31	443	1955
0.63	-0.081	1.640	0.2545	-0.00017	0.26	555	1378
0.79	0.080	1.693	0.2138	-0.00026	0.24	702	1140
1.00	0.262	1.577	0.0968	-0.00035	0.22	1313	1055
1.26	0.466	1.544	0.0325	-0.00045	0.22	1532	1004
1.59	0.624	1.515	0.0191	-0.00054	0.24	1620	1058
2.00	0.742	1.453	0.0058	-0.00063	0.25	1693	1161
2.51	0.902	1.411	-0.0104	-0.00080	0.26	1679	1155
3.16	1.003	1.329	-0.0160	-0.00096	0.27	1651	1219
3.98	1.101	1.250	-0.0211	-0.00118	0.28	1577	1250
5.01	1.204	1.198	-0.0198	-0.00144	0.29	1523	1284
6.31	1.255	1.115	-0.0200	-0.00164	0.31	1450	1425
7.94	1.298	1.035	-0.0095	-0.00185	0.32	1383	1588
10.00	1.337	0.946	-0.0173	-0.00204	0.32	1277	1811
12.59	1.315	0.905	0.0232	-0.00214	0.33	880	2176
15.85	1.320	0.827	0.0148	-0.00244	0.35	862	2401
19.95	1.167	0.682	-0.0366	-0.00271	0.49	821	2722

Values are in centimeters per second.

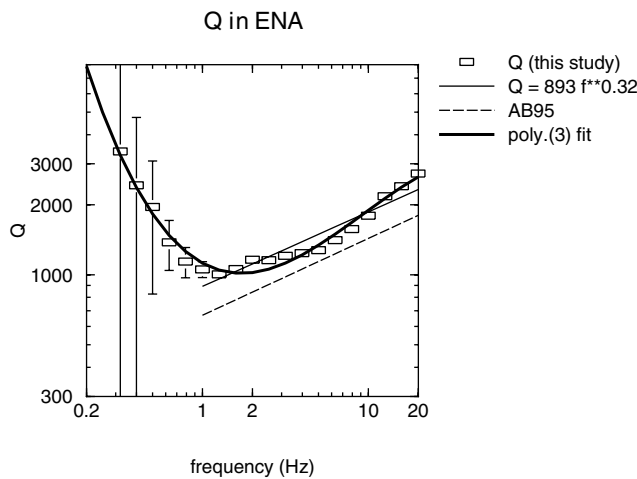


Figure 6.  $Q$  values determined from regression analysis (rectangles); error bars show standard error of  $Q$  based on standard error of  $c_4$  coefficient of the regression (error bars lie within symbol width at high frequencies). Heavy solid line shows polynomial fit to  $Q$  values. Light solid line shows linear fit to  $Q$  values. Dashed line shows  $Q$  model of Atkinson and Boore (1995).

the depth-corrected values of the Fourier acceleration spectrum.

In Figure 9, the residuals are plotted against magnitude; there are no apparent trends. I conclude that the attenuation model of equation (5) provides a satisfactory description of the vertical-component data. The fit may be improved by adding the focal-depth correction factors given by Table 3

to the predicted value, for cases where the focal depth of the event is known.

The residuals were averaged on a station-by-station basis to determine whether the relative vertical-component site response at any of the stations is significantly different from zero. A large average residual for a particular station would be indicative of significant site response. The residuals averaged by station show large variability among observations. As shown in Figure 10 for two frequencies (1 and 5 Hz), the standard deviations tend to be much larger than average residual values. Thus, although there may be some minor site response effects (especially at high frequencies), even for the vertical component, they do not appear to be very significant in relation to the overall data variability.

#### Horizontal-Component Attenuation Model

The horizontal-component database is not as rich in magnitude and distance as the vertical-component database. Rather than developing an independent attenuation model for the horizontal component, I apply the vertical-component model (equation 5) to the horizontal-component database, then examine the behavior of the residuals. If the residuals show no trends with distance (i.e., ratio of horizontal to vertical (H/V) does not depend on distance), then an independent attenuation model is not warranted for the horizontal component. It is generally believed that the ratio of the H/V component is a site parameter, controlled primarily by the near-surface attenuation (Bonilla *et al.*, 1987; Nakamura, 1989; Lermo and Chavez-Garcia, 1993; Theodulidis *et al.*, 1996; Seht and Wohlenberg, 1999; Atkinson and Cassidy, 2000; Siddiqi and Atkinson, 2002; Tsuboi *et al.*, 2001). The

Regression Residuals (transitions 70, 140 km:  $b_1=1.3$ ,  $b_2=-0.2$ )

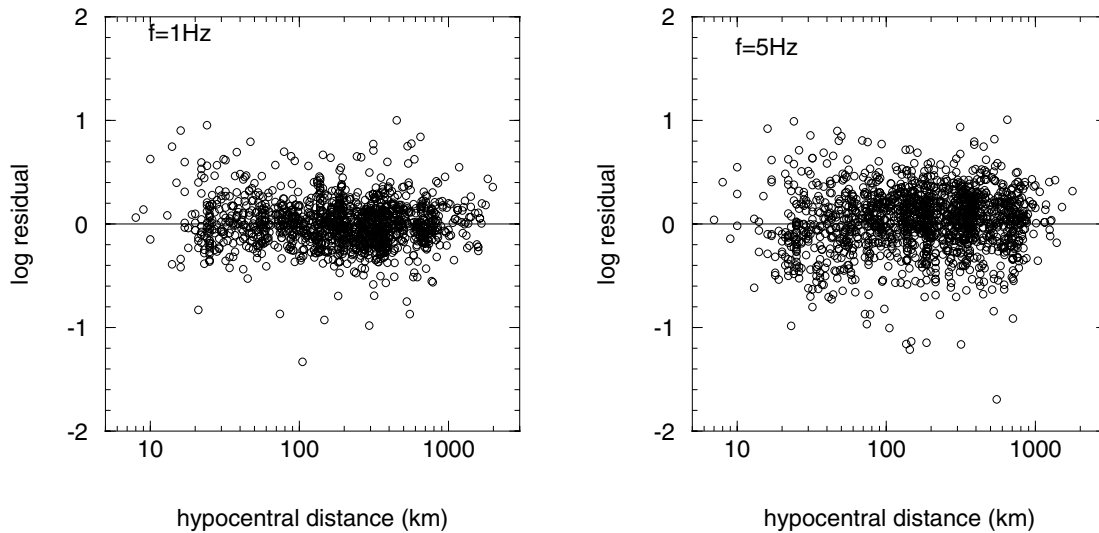


Figure 7. Log residuals (= log observed – log predicted Fourier acceleration) for the regression of vertical-component data versus distance, for frequencies of 1 and 5 Hz.

Table 3

Dependence of Regression Residuals on Focal Depth

Frequency (Hz)	$d_1$	$d_2$
<1.	0.	0.
1.	0.	0.
1.3	0.	0.
1.6	0.00034	0.002
2.	0.0007	0.008
2.5	0.0013	0.006
3.2	0.0025	0.004
4.	0.0034	0.002
5.	0.0042	-0.002
6.3	0.0048	-0.007
7.9	0.0055	-0.010
10.	0.0052	-0.021
12.	0.0043	-0.020
16.	0.0037	-0.010
20.	0.0033	-0.021

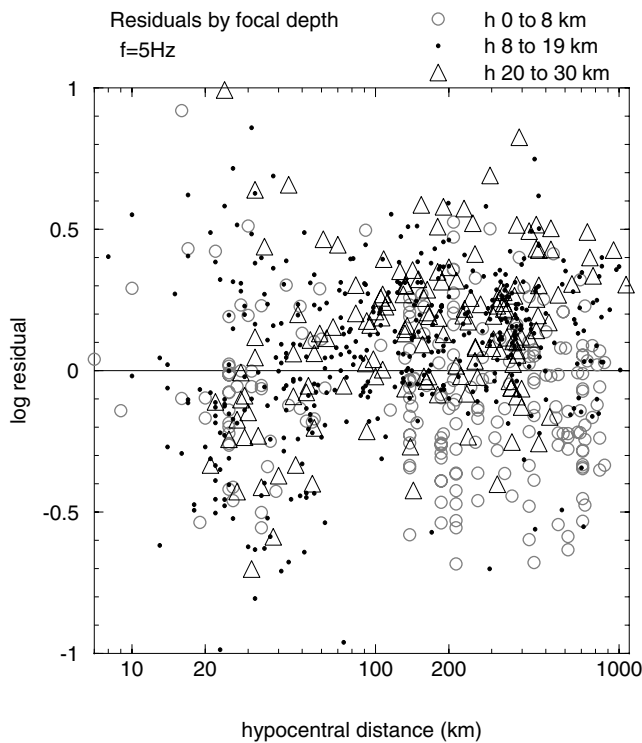


Figure 8. Examination of focal depth effects on residuals, for events with known focal depth, at 5 Hz. Large open circles plot residuals for shallow events ( $\leq 8$  km), small circles plot residuals for events of depth 8–19 km, and triangles plot residuals for events 20 km or more in depth.

The (log) Fourier amplitudes given by equation (5) may be corrected for the effect of focal depth by adding the factor  $\log \text{residual}(h) = d_1 (h - 10) \log R + d_2$ , where  $h$  = focal depth (km) and  $R$  is hypocentral distance (km).

horizontal component of motion is amplified by impedance gradients as the surface is approached, whereas this effect on the vertical component is counteracted by the refracting of rays toward the vertical in the velocity gradient. The net effect is that there is little amplification of the vertical component, making the H/V ratio a crude approximation of the near-surface amplification. For the hard-rock sites of the CNSN, near-surface amplification is modest. Correspondingly, the H/V ratio for rock sites in Canada is generally found to be near unity at 1 Hz, increasing gradually to values

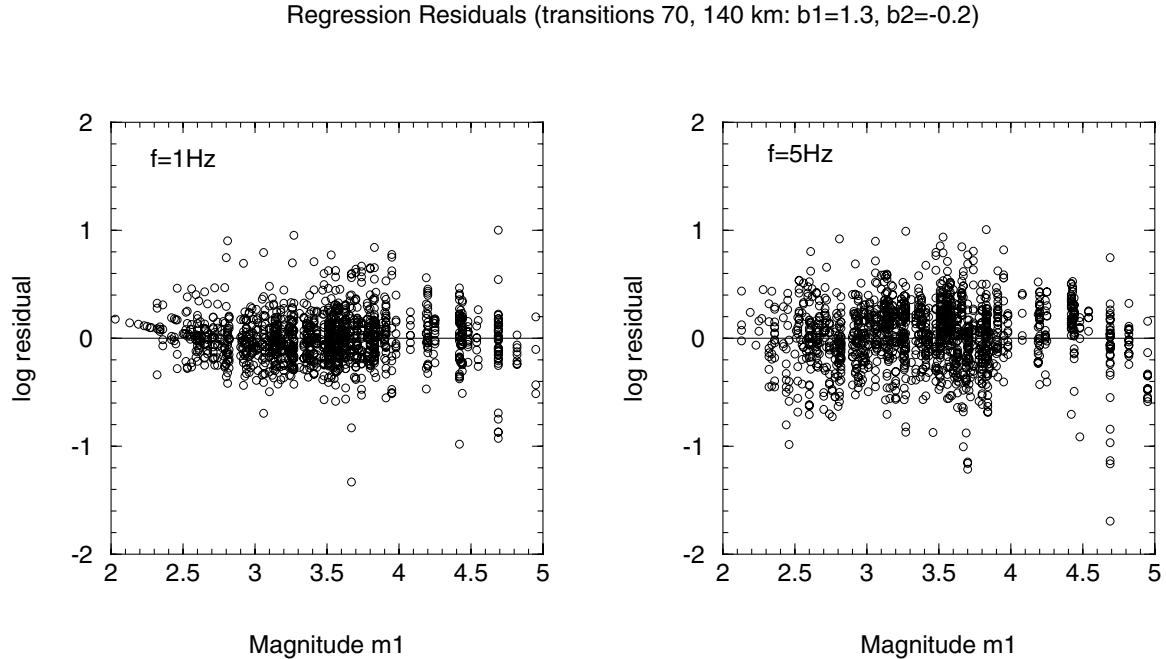


Figure 9. Log residuals (=log observed – log predicted Fourier acceleration) for the regression of vertical-component data versus magnitude  $m_1$ , for frequencies of 1 and 5 Hz.

of 1.2–1.5 at 10 Hz (Atkinson, 1993a; Siddiqi and Atkinson, 2002). This behavior is consistent with a shear-wave velocity profile that is characterized by near-surface values of about 2.8 km/sec, increasing to values of about 3.7 km/sec at seismogenic depths (Siddiqi and Atkinson, 2002).

Figure 11 shows the residuals that are obtained when horizontal-component motions are predicted using the vertical-component model of equation (5). Note that these residuals are also the log of the H/V ratio. No discernible trends with distance are seen. This is confirmed by statistical analysis, which indicates that the significance of any trend with distance is low; there is a slight positive distance trend to the log residuals of Figure 11, but the slope has a low value (about  $10^{-4}R$ ) and is not statistically significant at most frequencies. I therefore conclude that the H/V ratio is independent of distance and that the vertical-component attenuation model also describes the attenuation of the horizontal component. The horizontal residuals were also plotted versus focal depth, to verify that there are no depth trends in the H/V ratio. The H/V ratio that must be applied to equation (5) in order to predict horizontal-component motions is determined by plotting the mean log H/V (along with the standard error of the mean) as a function of frequency, as shown in Figure 12. There is a well-defined trend determined from the plotted points from frequencies 0.16 to 16 Hz, given by

$$\log H/V = 0.0234 + 0.106 \log f \quad (8)$$

(where the regression is performed on the points shown in

Fig. 12). The implied negative value of log H/V at  $f \leq 0.5$  Hz may not be meaningful, given the paucity of data at the lowest frequencies. The apparently low value of the H/V ratio at 20 Hz appears anomalous and may not be meaningful. The result, corresponding to an H/V ratio of about 1 at  $f \leq 1$  Hz, rising to about 1.35 at 10 Hz, is consistent with previous results of Atkinson (1993a) and Siddiqi and Atkinson (2002) for rock sites in eastern Canada.

#### Source Parameters (Moment $M$ , Stress Drop)

The attenuation model of equation (5) can be used to play back attenuation effects of each recorded earthquake in the database, which allows the apparent source spectrum to be determined for specific events, accounting for the focal depth of the event where known. For each recorded spectral amplitude ( $A$ ), an estimate of the corresponding apparent source spectrum  $A_0$  is obtained as

$$\log A_0 = \log A + 1.3 \log R + c_4 R - \log \text{residual}(h) \quad \text{for } R \leq 70 \text{ km}, \quad (9a)$$

$$\log A_0 = \log A + 1.3 \log (70) - 0.2 \log (R/70) + c_4 R - \log \text{residual}(h) \quad \text{for } 70 < R \leq 140 \text{ km}, \quad (9b)$$

$$\log A_0 = \log A + 1.3 \log (70) - 0.2 \log (140/70) + 0.5 \log (R/140) + c_4 R - \log \text{residual}(h) \quad \text{for } R > 140 \text{ km}, \quad (9c)$$

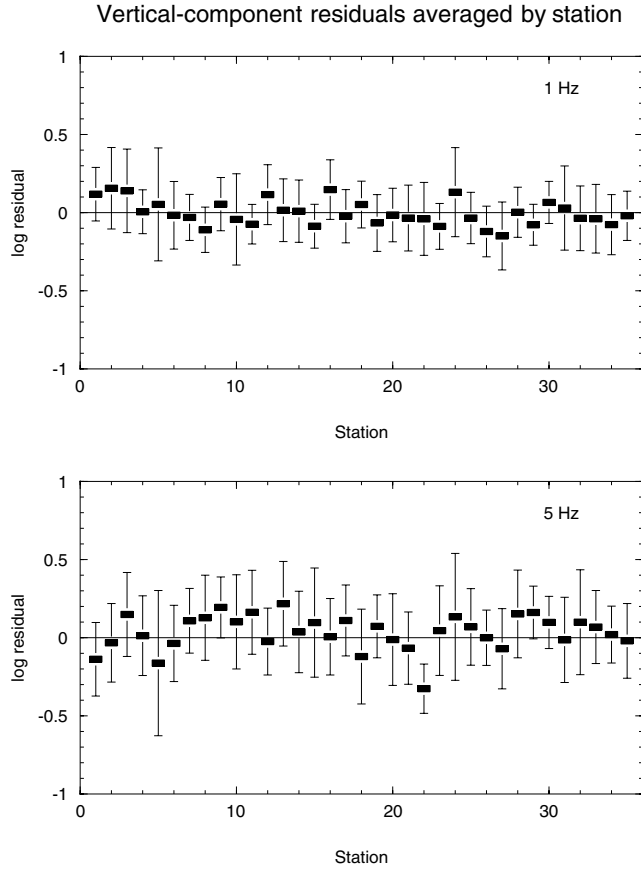


Figure 10. Average vertical-component residual and its standard deviation by station, at 1 and 5 Hz, for all stations having at least 10 observations. Station numbers correspond to station names as follows: 1, A11; 2, A16; 3, A21; 4, A54; 5, A61; 6, A64; 7, CKO; 8, CNQ; 9, CRLQ; 10, DAQ; 11, DPQ; 12, EBN; 13, EEO; 14, GAC; 15, GGN; 16, GNT; 17, GRQ; 18, GSQ; 19, HTQ; 20, ICQ; 21, KLN; 22, LMN; 23, LMQ; 24, LPQ; 25, MNQ; 26, MNT; 27, MOQ; 28, OTT; 29, SADO; 30, SBQ; 31, SCHQ; 32, SMQ; 33, TRQ; 34, VDQ; 35, WBO.

where  $\log \text{residual}(h)$  is the depth correction factor for the attenuation as given in Table 3. The apparent source spectrum for an event is determined by averaging the obtained source spectral amplitudes ( $\log A_0$ ) over all stations that recorded the event ( $\log$  average). The attenuation can be removed from either the vertical- or horizontal-component data using equation (9). Because the vertical-component data are more plentiful, and less influenced by near-surface amplification, they should provide a better estimate of the source spectrum. I therefore assume that the vertical-component spectra equal the horizontal-component spectra at the source and that the observed H/V ratio is representing near-surface amplification only (as opposed to a source effect). I therefore use the vertical-component data with equation (9) to determine the apparent source spectrum for each earthquake having at least three recordings. I assume that this equals the random horizontal-component spectrum at

the earthquake source (e.g., at  $R = 1$  km). (Note: An alternative would be to use the horizontal-component recordings corrected for both attenuation and average regional site effects for rock sites; this approach is equivalent but can only be applied to events having sufficient horizontal-component data.)

Figure 13 shows typical acceleration source spectra for events recorded on the broadband networks, for magnitudes  $m_1$  3.5–5, in comparison to the well-known Brune (1970, 1971) model point-source spectrum. The Brune model spectrum is plotted for a reference stress drop of 150 bars, which is a typical value for stress drops of moderate-to-large earthquakes in ENA (Atkinson, 1993b). The Brune model acceleration spectra are given by (Boore, 1983)

$$A_0 = CM_0 (2\pi f)^2 / [1 + (ff_0)^2], \quad (10)$$

where  $C = (0.55) (0.71) (2.) / (4 \pi \rho \beta^3)$ ,  $M_0$  is seismic moment, and  $f_0$  is the corner frequency. (Note: The constants in the numerator represent radiation pattern, partition onto two horizontal components, and free-surface amplification, respectively.) I assume  $\rho = 2.8 \text{ g/cm}^3$  and  $\beta = 3.7 \text{ km/sec}$  at seismogenic depths (near 10 km) (see Boore and Joyner, 1997; Atkinson and Boore, 1995). The corner frequency can be expressed as (Boore, 1983)

$$f_0 = 4.9 \times 10^6 \beta (\Delta\sigma/M_0)^{1/3} \quad (11)$$

for  $\Delta\sigma$  in bars,  $M_0$  in dyne centimeters, and  $\beta$  in kilometers per second. The Brune model shape matches the spectra well overall. Interestingly, though, the stress drop appears to be significantly less than 150 bars for events of  $m_1 < 4$ ; this is indicated by the fact that the high-frequency levels of the spectra for events of  $m_1$  3.5–4 fall below the range expected for a Brune model with a stress drop of 150 bars. This is not a bandwidth effect, as the high-frequency level is clearly resolved by the data.

The Brune model (equation 10) is used to determine the average value of seismic moment and stress drop for each event. The seismic moment is first determined for each event based on the long-period displacement spectral level at frequencies below the corner frequency (given by  $D_0 = CM_0$ ). In order to avoid the lowest frequency points, which are often unreliable, only the spectral amplitudes in the frequency range from  $f_0/2$  to  $f_0/5$  are used to determine the low-frequency spectral level. An initial estimate of  $f_0$  is made to define this frequency range by using equation (11), assuming that  $\Delta\sigma = 150$  bars,  $m_1 = \mathbf{M}$ , and  $\mathbf{M}$  is related to  $M_0$  by the definition of moment magnitude (Hanks and Kanamori, 1979). The determined values of  $M_0$  are not sensitive to the assumed stress drop used in determining the frequency limits over which to average the long-period spectral amplitudes, because the dependence of corner frequency on stress drop in equation (11) is weak.

With  $M_0$  determined from the long-period spectral level, the stress drop is then determined from the high-frequency

Horizontal-Component Residuals (transitions 70, 140km: b1=1.3, b2=-0.2)

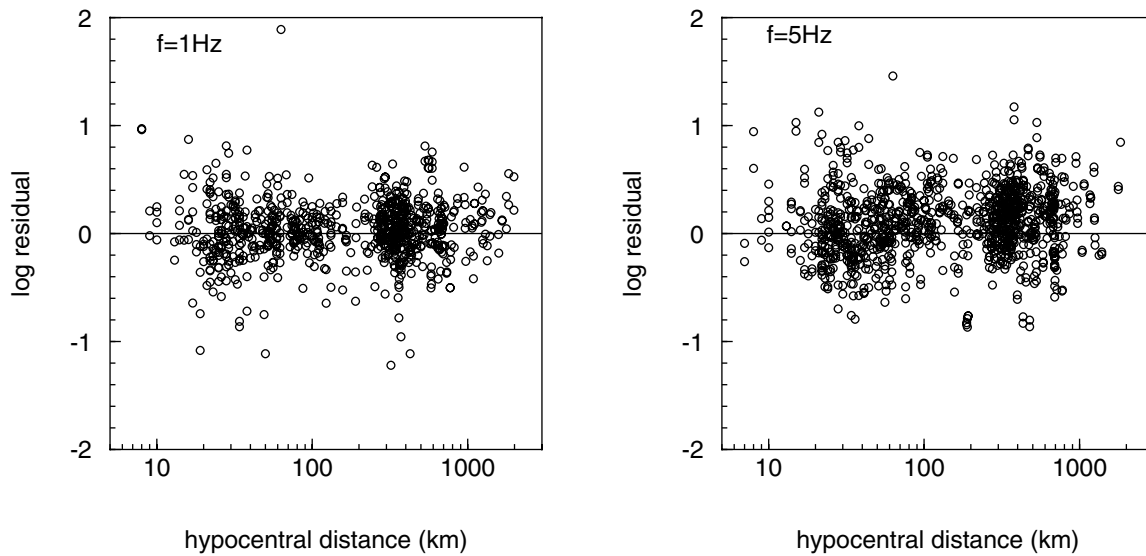


Figure 11. Log residuals (= log observed – log predicted Fourier acceleration) for the horizontal-component data versus distance, for frequencies of 1 and 5 Hz, obtained using the vertical-component regression equation to predict the horizontal-component motion. These residuals are the log of the H/V ratio.

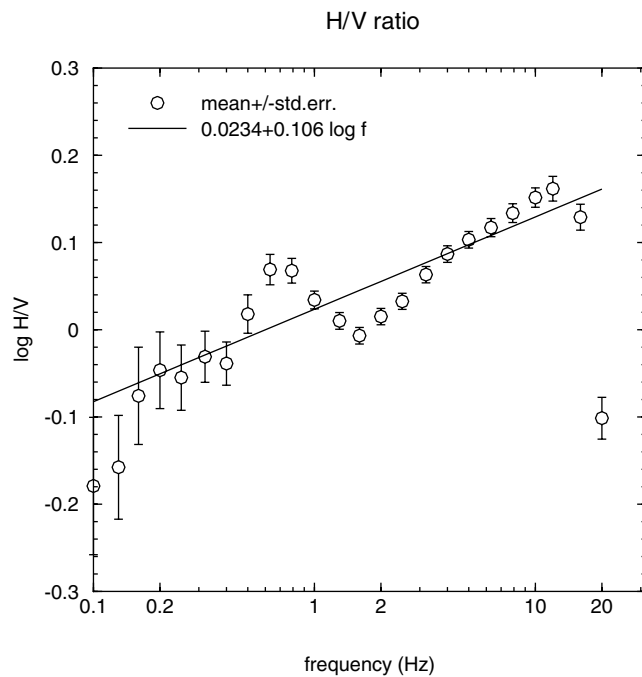


Figure 12. Mean log H/V ratio and its standard error as a function of frequency (symbols). Line shows fit to H/V ratio for frequencies from 0.16 to 16 Hz.

spectral level. Using the spectral acceleration amplitudes for frequencies greater than the preliminary estimate of  $f_0$ , the average level of the high-frequency spectrum is obtained. From equation (10), this level ( $A_0$  for  $f \gg f_0$ ) can be expressed as  $A_{0_{max}} = CM_0 4\pi^2 f_0^2$ , from which the actual corner frequency of the spectrum can then be calculated. If the actual value of  $f_0$  is greater than the initial estimate, I repeat the process to determine the high-frequency spectral level, using the higher value of  $f_0$  as the new lower cut off on frequencies included in the spectral averaging, until it is determined that only spectral values above the actual corner frequency were used to define the high-frequency level and hence determine  $f_0$ . The stress drop is not determined unless there are at least three spectral data points that lie above the corner frequency; this ensures that a stable high-frequency level is obtained that includes spectral content well above the corner frequency. Visual inspection of many events was used to verify that these procedures resulted in reliable interpretation of both the high- and low-frequency spectral levels. For many of the smallest events, there is insufficient bandwidth at the high-frequency end of the spectrum to determine the high-frequency spectral level; in the estimation procedure outlined earlier, the estimate of  $f_0$  continues to grow with iteration until it exceeds the available bandwidth. In such cases, the stress drop cannot be determined.

Table 4 lists the determined values of moment magnitude and stress drop for all study events with three or more recordings. There are 14 events for which moment magnitudes are available from independent waveform modeling

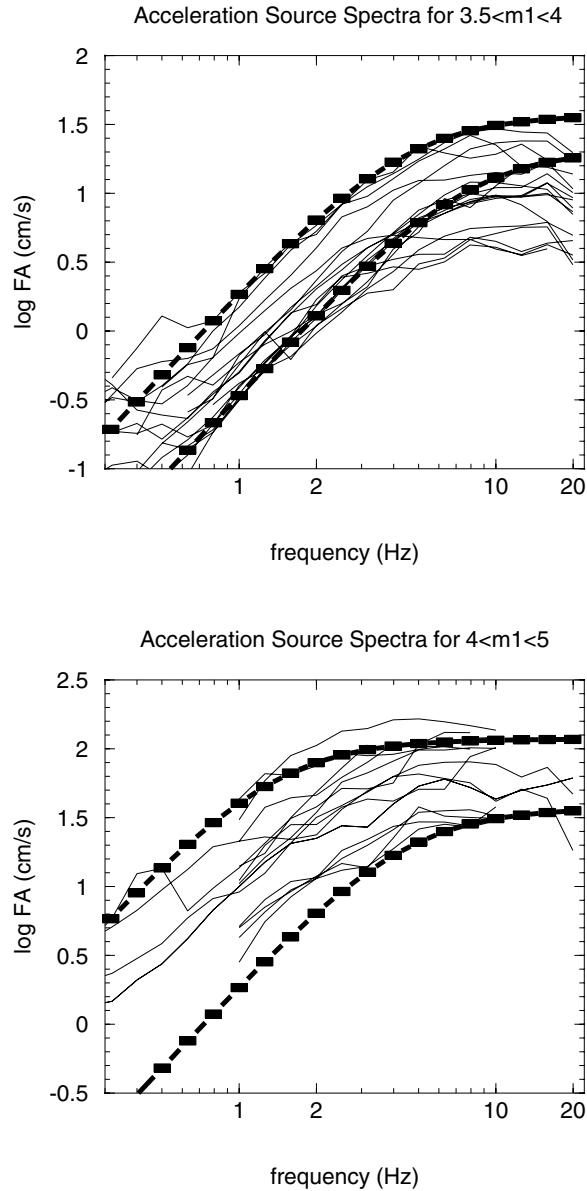


Figure 13. Acceleration source spectra (light lines) for post-1995 study earthquakes (with broadband data). Top frame shows events of  $3.5 \leq m_1 < 4$  in comparison to Brune model spectra (heavy lines with symbols) for a stress drop of 150 bars for  $M$  3.5 and 4. Lower frame shows events of  $4 \leq m_1 < 5$  in comparison to Brune model spectra (heavy lines with symbols) for a stress drop of 150 bars for  $M$  4 and 5.

studies (Atkinson and Boore, 1995; A. Bent, 2003, personal comm.; Du *et al.*, 2003). Figure 14 compares the  $M$  estimates of this study with the independent estimates based on waveform modeling. Most of my moment magnitude estimates are within 0.2 units of the established values; the average difference is 0.007 units, with a standard deviation of 0.16 magnitude units. Thus the use of regional seismographic data, corrected for empirical attenuation, is a reasonably reliable method of estimating moment magnitude.

Table 4  
Source Parameters for Study Events

Date (yyyy mm dd)	$m_1$	Depth	$f$	$n_{\text{sta}}$	$M$	$\Delta\sigma$ (bars)	$f_0$ (Hz)	$\Delta\sigma$ (min)
1980 03 11	3.58	10.0	1	5	3.53	77.0	5.93	
1981 06 16	3.36	8.0	0	6	3.29	—	8.99	44.8
1981 07 04	3.51	13.0	0	9	3.40	44.7	5.75	
1981 09 18	3.25	10.0	1	10	3.20	—	10.21	34.9
1981 09 30	3.26	10.0	1	10	3.14	—	10.09	34.0
1981 11 28	3.61	5.0	0	3	3.55	—	6.74	9.9
1982 01 09	3.72	5.0	0	3	3.60	—	5.94	14.6
1982 01 09	3.72	5.0	0	4	3.57	—	5.94	5.3
1982 01 11	4.95	5.0	0	14	4.95	123.3	1.35	
1982 01 13	3.50	5.0	0	6	3.38	—	7.65	7.3
1982 01 17	3.59	5.0	0	4	3.47	—	6.90	6.5
1982 01 19	4.08	7.0	0	8	4.14	106.9	3.26	
1982 03 16	3.48	5.0	0	5	3.40	8.8	3.35	
1982 03 31	4.24	5.0	0	13	4.23	83.7	2.71	
1982 04 02	3.85	5.0	0	11	3.82	30.2	3.12	
1982 04 11	3.84	5.0	0	11	3.76	53.2	4.03	
1982 04 18	3.84	5.0	0	11	3.71	27.4	3.44	
1982 05 06	3.62	5.0	0	9	3.62	31.4	3.97	
1982 06 16	4.19	8.0	0	15	4.21	66.4	2.57	
1982 06 23	3.05	10.0	1	8	3.05	—	12.85	32.0
1982 07 13	3.43	10.0	1	8	3.37	38.4	5.61	
1982 07 28	3.62	5.0	0	5	3.52	—	6.67	5.6
1982 08 06	3.18	10.0	1	9	3.24	—	11.06	38.0
1982 08 13	3.66	10.0	1	6	3.70	117.2	5.62	
1982 09 03	3.43	10.0	1	6	3.34	40.1	5.91	
1982 10 26	3.24	5.0	0	5	3.22	—	10.32	9.0
1982 12 04	3.51	15.0	0	10	3.49	74.7	6.18	
1983 01 17	3.82	10.0	1	11	3.80	74.0	4.29	
1983 05 13	3.31	5.0	0	4	3.28	—	9.52	15.7
1983 05 13	3.90	5.0	0	5	3.91	46.3	3.23	
1983 05 16	3.55	11.0	0	11	3.55	43.2	4.78	
1983 05 29	3.80	2.0	0	15	3.86	55.8	3.68	
1983 08 12	3.17	10.0	1	4	3.19	—	11.19	5.3
1983 10 07	4.82	4.0	0	16	4.82	313.8	2.14	
1983 10 07	3.38	13.0	0	8	3.39	70.8	6.80	
1983 10 11	3.78	14.0	0	12	3.77	43.0	3.73	
1983 11 17	3.47	5.0	0	5	3.46	—	7.92	11.9
1983 12 28	3.10	10.0	1	7	3.06	—	12.13	25.7
1984 02 24	3.56	5.0	0	7	3.50	26.5	4.34	
1984 04 11	3.60	10.0	1	5	3.55	40.8	4.70	
1984 09 23	3.60	10.0	1	4	3.50	—	6.82	7.8
1984 11 30	3.78	5.0	0	5	3.64	19.0	3.29	
1985 03 03	3.13	14.0	0	3	2.95	—	11.72	7.7
1985 04 12	3.16	9.0	0	8	3.10	—	11.32	41.6
1985 10 05	3.69	5.0	0	15	3.62	16.9	3.25	
1985 10 19	3.88	10.0	1	8	3.85	28.5	2.94	
1986 01 11	3.59	6.4	0	11	3.54	53.5	5.22	

(continued)

Figure 15 shows the dependence of stress drop on moment magnitude for the events from this study. Atkinson (1993b) noted that the stress drop increases with magnitude until about  $M$  4, above which it appears to have a relatively constant value in the range of 100–200 bars. The results of this study are consistent with that observation, although a constant stress level is not attained until  $M \geq 4.3$ . It appears that the low stress drops for small events really do reflect low high-frequency spectral amplitudes, not a bandwidth

Table 4  
Continued

Date (yyyy mm dd)	$m_1$	Depth	$f$	$n_{\text{stn}}$	<b>M</b>	$\Delta\sigma$ (bars)	$f_0$ (Hz)	$\Delta\sigma$ (min)
1986 01 31	4.69	10.0	1	14	4.69	158.8	1.98	
1986 07 12	4.48	10.0	1	15	4.50	119.7	2.23	
1986 08 06	3.39	10.0	1	8	3.32	14.6	4.32	
1986 09 19	3.74	22.0	0	16	3.73	37.0	3.71	
1986 11 09	3.83	10.0	1	14	3.83	36.0	3.26	
1987 08 06	2.99	10.0	1	3	3.02	—	13.77	11.5
1987 09 26	3.48	5.0	1	6	3.42	38.1	5.30	
1987 10 23	3.34	14.0	0	6	3.29	50.5	6.84	
1987 11 11	3.26	17.0	0	14	3.17	—	10.09	41.6
1988 01 02	3.24	11.0	0	8	3.21	—	10.32	14.4
1988 01 28	3.69	10.0	1	10	3.62	6.2	2.29	
1988 03 10	3.37	12.0	0	6	3.36	96.4	7.77	
1988 03 13	2.96	6.0	0	9	2.84	—	14.25	14.9
1988 04 24	3.49	5.0	1	4	3.41	12.2	3.69	
1988 05 09	3.34	5.0	1	9	3.23	—	9.20	7.4
1988 05 15	3.01	8.0	0	4	3.01	—	13.45	14.2
1988 08 09	3.07	9.0	0	6	2.97	—	12.56	27.6
1988 08 26	3.63	5.0	1	8	3.57	—	6.59	9.8
1988 10 20	3.56	5.0	1	7	3.55	—	7.14	10.5
1988 11 23	4.25	29.0	0	12	4.26	77.0	2.55	
1988 11 26	3.58	26.0	0	21	3.57	90.0	6.00	
1989 01 19	3.37	25.0	0	9	3.30	42.7	6.37	
1989 01 31	2.98	19.0	0	6	2.84	—	13.93	21.5
1989 02 10	3.90	10.0	1	5	3.91	54.6	3.41	
1989 03 09	3.79	10.0	1	8	3.78	33.1	3.36	
1989 08 10	3.51	5.0	0	9	3.36	—	7.57	7.9
1989 10 13	3.27	22.0	0	7	3.15	22.6	6.15	
1989 11 04	2.73	7.0	0	3	2.76	—	18.57	18.0
1989 11 16	3.52	10.0	1	14	3.57	41.9	4.63	
1989 11 22	3.16	8.0	0	7	3.07	—	11.32	18.8
1989 12 25	4.55	5.0	0	14	4.57	205.2	2.47	
1990 03 03	3.43	20.0	0	10	3.41	36.2	5.34	
1990 03 13	2.99	15.0	0	7	2.83	—	13.77	17.8
1990 04 21	3.01	9.0	0	7	2.88	—	13.45	16.3
1990 04 23	2.81	7.0	0	8	2.72	—	16.94	16.1
1990 10 07	3.54	13.0	0	4	3.51	39.3	4.88	
1990 10 19	4.46	13.0	0	10	4.49	267.7	2.99	
1990 10 21	2.98	15.0	0	7	2.92	—	13.93	36.8
1990 12 18	3.06	9.0	0	7	2.94	—	12.70	11.2
1997 11 06	4.20	22.5	0	25	4.22	96.5	2.87	
1998 06 17	2.52	18.0	1	4	2.41	—	23.65	9.5
1998 07 13	2.92	18.0	1	4	2.85	64.3	12.21	
1998 07 15	3.80	5.0	1	20	3.76	8.6	2.19	
1998 07 30	2.52	10.0	1	4	2.24	95.2	4.03	
1998 07 30	3.91	10.0	1	25	3.93	—	23.65	10.4
1998 08 08	2.66	18.0	1	3	2.57	—	20.13	31.9
1998 09 18	3.15	18.0	1	11	3.07	49.2	8.65	
1998 09 25	4.54	5.0	1	5	4.76	134.7	1.72	
1998 09 29	2.42	18.0	1	4	2.42	—	26.54	25.0
1998 10 05	2.34	18.0	1	4	2.12	—	29.10	9.0
1998 10 21	2.46	9.8	0	7	2.14	—	25.34	8.9
1998 10 22	3.57	18.0	1	24	3.50	47.5	5.24	
1998 12 25	3.02	18.0	1	10	2.99	11.7	5.87	
1999 01 19	2.82	18.0	1	9	2.69	23.1	10.39	
1999 01 22	3.26	18.0	1	13	3.12	57.7	8.58	
1999 02 23	2.78	18.0	1	8	2.51	19.2	12.10	
1999 02 26	3.63	18.0	1	11	3.58	13.2	3.12	
1999 03 08	2.60	12.0	0	5	2.44	—	21.57	16.5
1999 03 09	2.82	10.0	1	7	2.67	13.1	8.86	
1999 03 15	2.58	18.0	1	4	2.45	—	22.07	21.8

(continued)

Table 4  
Continued

Date (yyyy mm dd)	$m_1$	Depth	$f$	$n_{\text{stn}}$	<b>M</b>	$\Delta\sigma$ (bars)	$f_0$ (Hz)	$\Delta\sigma$ (min)
1999 03 16	4.44	19.0	0	27	4.50	104.4	2.16	
1999 03 17	2.82	18.0	1	3	2.53	20.9	12.11	
1999 03 25	2.65	18.0	1	8	2.66	—	20.36	32.2
1999 06 18	3.07	22.0	0	15	3.00	28.6	7.90	
1999 07 26	2.74	20.5	0	7	2.44	14.1	11.74	
1999 07 29	2.76	18.0	1	3	2.30	17.7	14.89	
1999 08 15	2.25	23.0	0	3	2.25	—	32.27	18.8
1999 10 02	2.70	18.0	1	3	2.27	14.5	9.65	
1999 10 02	2.80	8.7	0	8	2.62	17.2	15.29	
1999 10 28	2.66	15.3	0	5	2.43	—	20.13	10.3
1999 10 31	3.51	16.0	0	19	3.44	53.9	5.83	
1999 11 26	3.24	5.0	1	7	3.20	54.9	7.78	
1999 12 21	2.62	17.0	0	6	2.54	—	21.08	7.2
2000 01 01	4.42	13.0	0	33	4.54	143.2	2.27	
2000 01 03	3.41	1.0	1	10	3.27	9.2	3.93	
2000 01 08	2.61	18.0	1	3	2.48	—	21.32	13.0
2000 01 15	2.81	24.0	0	7	2.52	25.5	13.13	
2000 01 17	3.51	10.0	1	11	3.42	25.1	4.61	
2000 01 23	2.36	8.7	0	8	2.25	—	28.43	9.6
2000 02 07	2.45	18.0	1	4	2.56	—	25.63	34.0
2000 02 07	2.71	18.0	1	4	2.67	63.8	14.93	
2000 02 09	2.60	13.1	0	6	2.12	—	21.57	6.6
2000 03 02	2.81	12.0	0	6	2.68	22.1	10.36	
2000 03 20	2.91	15.0	0	6	2.87	27.9	9.05	
2000 04 05	2.94	18.0	1	7	2.72	22.2	9.89	
2000 04 20	3.71	18.0	1	20	3.68	21.8	3.29	
2000 06 15	3.38	11.4	0	14	3.30	72.0	7.62	
2000 06 29	2.94	18.0	1	9	2.92	43.5	9.85	
2000 07 03	2.44	11.6	0	7	2.09	—	25.93	7.7
2000 07 11	2.34	18.0	1	3	2.30	—	29.10	8.3
2000 07 12	3.66	18.0	1	21	3.64	130.6	6.19	
2000 07 12	3.14	18.0	1	6	3.11	141.1	11.75	
2000 08 06	3.63	18.0	1	24	3.60	14.1	8.62	
2000 08 06	2.97	18.0	1	4	2.71	46.4	4.59	
2000 08 16	2.32	15.7	0	7	2.14	—	29.77	7.0
2000 09 21	2.55	7.4	0	4	2.36	—	22.85	19.9
2000 09 27	2.92	8.1	0	8	2.84	70.2	12.74	
2000 10 06	3.18	18.0	1	10	3.20	42.9	7.11	
2000 10 10	2.60	18.0	0	7	2.47	—	21.57	19.2
2000 10 23	2.13	18.0	1	4	2.21	—	37.05	8.3
2000 11 10	2.67	18.0	1	7	2.73	39.8	11.98	
2001 01 14	2.93	18.0	1	8	2.75	25.0	9.96	
2001 01 26	3.98	5.0	1	10	4.03	56.3	3.01	
2001 02 06	2.71	12.0	0	8	2.74	44.1	12.21	
2001 03 19	3.36	21.0	0	5	3.36	41.9	5.94	
2001 03 24	3.95	18.0	1	15	3.92	68.1	3.62	
2001 04 11	3.13	22.0	0	12	3.09	24.6	6.72	
2001 05 22	3.67	10.9	0	12	3.61	62.5	5.08	
2001 06 12	2.94	18.0	1	5	2.97	24.9	7.76	
2001 07 27	3.10	18.0	1	7	3.12	47.7	8.10	
2001 08 18	2.65	18.0	1	5	2.51	—	20.36	34.6
2001 09 15	3.58	5.0	1	3	3.52	12.04	3.24	
2001 09 16	3.43	5.0	1	5	3.30	13.6	4.31	
2001 11 10	2.72	25.0	0	6	2.66	9.4	8.03	
2001 11 14	2.60	18.0	1	5	2.67	—	21.57	15.7
2001 11 15	2.59	15.0	0	5	2.60	—	21.82	9.3
2001 12 24	3.14	13.0	0	9	3.19	51.3	7.71	
2002 01 20	3.52	30.0	1	20	3.48	63.5	5.90	
2002 02 11	3.41	10.0	1	16	3.32	64.1	7.09	
2002 02 24	2.61	18.0	1	5	2.66	—	21.32	16.0

(continued)

Table 4  
Continued

Date (yyyy mm dd)	$m_1$	Depth	$f$	$n_{\text{stn}}$	$M$	$\Delta\sigma$ (bars)	$f_0$ (Hz)	$\Delta\sigma$ (min)
2002 04 01	2.74	13.0	0	6	2.67	14.8	9.23	
2002 04 20	4.69	12.0	0	32	4.84	48.3	1.12	
2002 04 20	2.82	18.0	1	7	2.66	14.1	3.27	
2002 04 20	3.70	18.0	1	10	3.55	3.1	5.55	
2002 04 25	2.67	18.0	1	3	2.55	46.0	15.41	
2002 04 27	2.56	19.0	0	5	2.56	—	22.59	15.2
2002 05 03	2.36	18.0	1	5	2.41	—	28.43	11.4
2002 05 14	2.90	14.1	0	8	2.77	36.2	11.12	
2002 05 24	3.20	10.0	1	11	3.13	14.6	5.40	
2002 05 28	3.20	18.0	1	8	2.98	17.4	6.80	
2002 06 01	2.53	18.0	1	9	2.68	—	23.38	26.3
2002 06 05	3.83	5.0	1	40	3.84	45.0	3.45	
2002 06 12	2.79	7.8	0	8	2.77	38.5	11.23	
2002 06 25	3.15	10.0	1	5	3.01	7.8	5.02	
2002 07 23	3.53	18.0	1	22	3.50	50.0	5.33	
2002 08 17	3.27	13.3	0	15	3.24	80.1	8.38	
2002 08 24	3.14	18.0	1	5	2.82	4.2	5.11	
2002 09 07	3.12	23.0	0	15	3.08	27.2	7.09	
2003 06 13	3.56	11.5	0	26	3.52	53.7	5.32	

Focal depth in kilometer; depth is assigned (unknown) where indicated by  $f = 1$ .

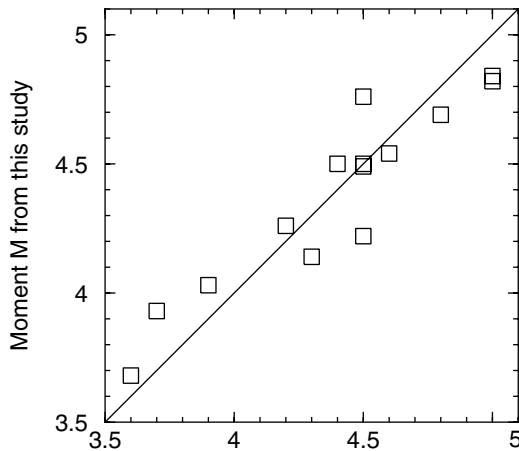
Abbreviations:  $n_{\text{stn}}$ , number of stations;

$\Delta\sigma$ , stress drop in bars;

$f_0$ , corner frequency;

$\Delta\sigma(\text{min})$ , minimum stress drop in cases where apparent corner frequency lies above the available bandwidth.

Moment magnitude comparison



Moment M from waveform modeling

Figure 14. Comparison of moment magnitude estimates determined in this study, by correcting observed spectra for regional attenuation effects, to independent moment magnitudes determined from waveform modeling studies.

ENA Stress Drop  
( $n_a \geq 3$ )

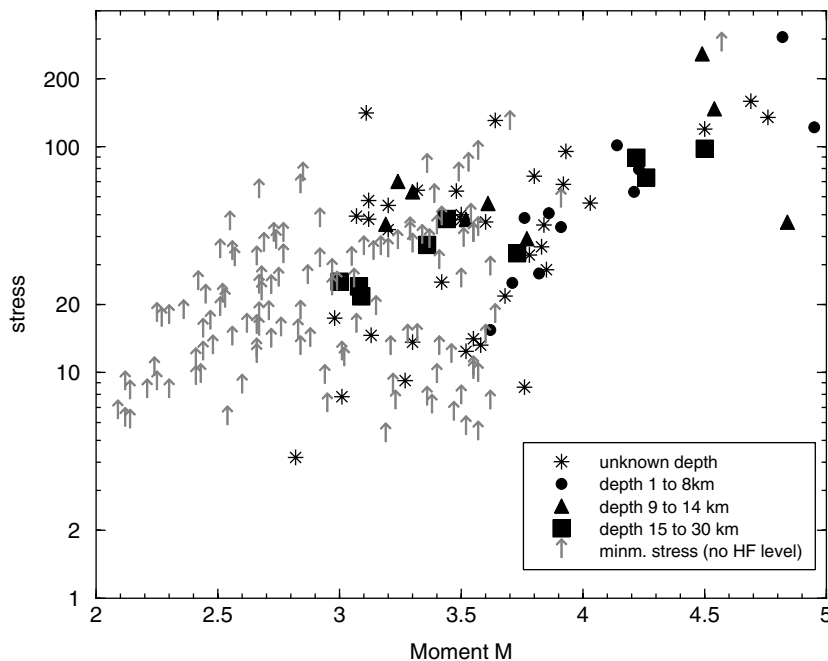


Figure 15. Brune stress drop based on high-frequency spectral level, for events having at least three spectral frequencies available above the corner frequency, versus moment magnitude. Symbols distinguish between focal depths where known.

limitation, as the high-frequency levels can be clearly seen for events of magnitude 3.5–4 on Figure 13. Furthermore, the stress drops are not plotted on Figure 15 unless at least three spectral amplitude values are available above the determined corner frequency. Stress drop does not appear to depend on depth.

Figure 16 plots magnitude  $m_1$  versus moment magnitude. This confirms that  $m_1$  is an excellent estimate of  $\mathbf{M}$  for  $\mathbf{M} < 4.5$ , despite a small offset from the 1:1 relationship at small magnitudes. Over the magnitude range plotted, the average difference between  $m_1$  and  $\mathbf{M}$  is 0.07 units, with a standard deviation of 0.10 units. For the purpose of using equation (5) to predict Fourier spectral amplitudes for events of  $\mathbf{M}$  3–5 for which the moment magnitude is known,  $m_1$  can be estimated using the least-squares relation

$$m_1 = 0.36 + 0.91\mathbf{M}. \quad (12)$$

At larger magnitudes ( $\mathbf{M} > 5$ ), it is expected that  $m_1$  will deviate from  $\mathbf{M}$  due to finite fault effects that introduce complexity in the spectral shape (Chen and Atkinson, 2002).

### Conclusions

Regression analysis of 1700 digital seismograms has determined that Fourier spectral amplitudes for the shear window, for the vertical and horizontal component of motion, for earthquakes of moment magnitude 2.5–5 in south-

eastern Canada and the northeastern United States follow a hinged trilinear attenuation model. Spectral amplitudes decay as  $R^{-1.3}$  within 70 km of the source. There is a transition zone from 70 to 140 km, as the direct waves are joined by strong postcritical reflections, where the attenuation is described as  $R^{+0.2}$ . Beyond 140 km, the attenuation is well described by  $R^{-0.5}$ . The associated model for the regional quality factor for frequencies greater than 1 Hz can be expressed as  $Q = 893f^{0.32}$ .  $Q$  can be better modeled over a wider frequency range (0.2–20 Hz) by a polynomial expression:  $\log Q = 3.052 - 0.393 \log f + 0.945 (\log f)^2 - 0.327 (\log f)^3$ . The attenuation model can be refined for events of known focal depth using correction factors developed from analysis of the ground-motion database (Table 3).

Correction of regional seismographic data for the observed attenuation effects can be used to estimate the spectrum of ground motion in the shear window near the earthquake source. The apparent source spectra of earthquakes of  $2.5 \leq \mathbf{M} \leq 5$  are well described by the Brune (1970, 1971) source model. From the long-period level of the spectrum, the moment magnitude can be estimated. Estimates of moment magnitude obtained this way are consistent with independent estimates based on waveform modeling. A simple regional magnitude measure,  $m_1$ , also provides a good estimate of  $\mathbf{M}$  for small earthquakes ( $\mathbf{M} < 5$ ). The high-frequency level of the source spectrum may be used to estimate the Brune stress drop. Stress drop increases with moment magnitude for events of  $\mathbf{M} < 4.3$ , then appears to attain a relatively constant level in the range from 100 to 200 bars for the larger events, as previously noted by Atkinson (1993b).

The results of this study provide a useful framework for improving regional ground motion relations in ENA. They further our understanding of attenuation in the region through analysis of a large ground-motion database. In particular, the inclusion of the three-component broadband data gathered over the last decade allows extension of attenuation models to both horizontal and vertical components over a broad frequency range (0.2–20 Hz).

### Acknowledgments

Thanks to those that assisted with data processing of CNSN and USNSN data over the last few years: Raymond Casey, Eleanor Sonley, Aaron Snider, San Linn Kaka, Jamila Siddiqi, and Shutian Ma. This study was supported by the National Hazards and Earthquake Reduction Program under Grant Number 02HQGR0001 and by the Natural Sciences and Engineering Research Council of Canada. All graphics were produced using COPLLOT ([www.cohort.com](http://www.cohort.com)).

Data from the CNSN were obtained by autodrm (the Automatic Data Request Manager) from the Geological Survey of Canada ([www.seismo.nrcan.gc.ca](http://www.seismo.nrcan.gc.ca)) over the time period from 1998 to 2003. Data from the U.S. National Seismic Network were obtained from the IRIS autodrm ([www.iris.edu](http://www.iris.edu)), 2003. ECTN data are from the Geological Survey of Canada, 1990, as reported in Atkinson and Mereu (1992).

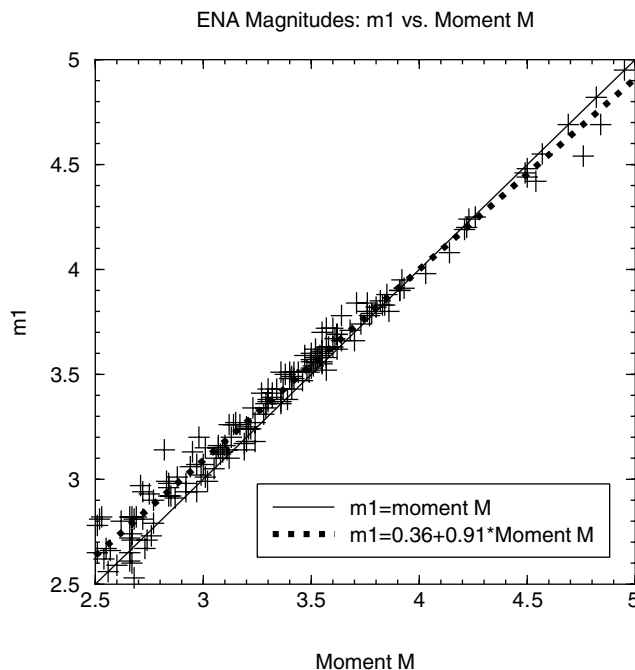


Figure 16. 1-Hz magnitude  $m_1$  versus moment magnitude for the study earthquakes. Solid line shows 1:1 relation; dotted line shows best-fit relation.

## References

- Aki, K. (1980). Attenuation of shear waves in the lithosphere for frequencies from 0.05 to 25 Hz, *Phys. Earth Planet. Inter.* **21**, 50–60.
- Atkinson, G. (1993a). Notes on ground motion parameters for eastern North America: duration and H/V ratio, *Bull. Seism. Soc. Am.* **83**, 587–596.
- Atkinson, G. (1993b). Source spectra for earthquakes in eastern North America, *Bull. Seism. Soc. Am.* **83**, 1778–1798.
- Atkinson, G., and D. Boore (1995). New ground motion relations for eastern North America, *Bull. Seism. Soc. Am.* **85**, 17–30.
- Atkinson, G., and J. Cassidy (2000). Integrated use of seismograph and strong motion data to determine soil amplification in the Fraser Delta: results from the Duvall and Georgia Strait earthquakes, *Bull. Seism. Soc. Am.* **90**, 1028–1040.
- Atkinson, G., and R. Mereu (1992). The shape of ground motion attenuation curves in southeastern Canada, *Bull. Seism. Soc. Am.* **82**, 2014–2031.
- Beresnev, I., and G. Atkinson (1997). Shear wave velocity survey of seismographic sites in eastern Canada: calibration of empirical regression method of estimating site response, *Seism. Res. Lett.* **68**, 981–987.
- Bonilla, L., J. Steidl, G. Lindley, A. Tumarkin, and R. Archuleta (1997). Site amplification in the San Fernando Valley, California: variability of site-effect estimation using the S-wave, coda, and H/V methods, *Bull. Seism. Soc. Am.* **87**, 710–730.
- Boore, D. (1983). Stochastic simulation of high-frequency ground motions based on seismological models of the radiated spectra, *Bull. Seism. Soc. Am.* **73**, 1865–1894.
- Boore, D. (2003). Simulation of ground motion using the stochastic method, *Pure Appl. Geophys.* **160**, 636–676.
- Boore, D., and W. Joyner (1997). Site amplifications for generic rock sites, *Bull. Seism. Soc. Am.* **87**, 327–341.
- Bowman, J., and B. Kennett (1991). Propagation of Lg waves in the North Australian craton: influence of crustal velocity gradients, *Bull. Seism. Soc. Am.* **81**, 592–610.
- Brune, J. (1970). Tectonic stress and the spectra of seismic shear waves from earthquakes, *J. Geophys. Res.* **75**, 4997–5009.
- Brune, J. (1971). Correction, *J. Geophys. Res.* **76**, 5002.
- Burger, R., P. Somerville, J. Barker, R. Herrmann, and D. Helmberger (1987). The effect of crustal structure on strong ground motion attenuation relations in eastern North America, *Bull. Seism. Soc. Am.* **77**, 420–439.
- Campbell, K. (2003). Prediction of strong-ground motion using the hybrid-empirical method and its use in the development of ground-motion (attenuation) relations in eastern North America, *Bull. Seism. Soc. Am.* **93**, 1012–1033.
- Chen, S., and G. Atkinson (2002). Global comparisons of earthquake source spectra, *Bull. Seism. Soc. Am.* **92**, 885–895.
- Chun, K., G. West, R. Kokoski, and C. Samson (1987). A novel technique for measuring Lg attenuation—Results from eastern Canada between 1 and 10 Hz., *Bull. Seism. Soc. Am.* **77**, 398–419.
- Cormier, V. (1982). The effect of attenuation on seismic body waves, *Bull. Seism. Soc. Am.* **72**, S169–S200.
- Du, W., W. Kim, and L. Sykes (2003). Earthquake source parameters and state of stress for the northeastern United States and southeastern Canada from analysis of regional seismograms, *Bull. Seism. Soc. Am.* **93**, 1633–1648.
- Frankel, A., C. Mueller, T. Barnhard, D. Perkins, E. Leyendecker, N. Dickman, S. Hanson, and M. Hopper (1999). National seismic hazard mapping project, <http://geohazards.cr.usgs.gov> (last accessed August, 2003).
- Hanks, T., and H. Kanamori (1979). A moment magnitude scale, *J. Geophys. Res.* **84**, 2348–2350.
- Herrmann, R., and A. Kijko (1983). Modeling some empirical vertical component Lg relations, *Bull. Seism. Soc. Am.* **73**, 157–171.
- Herrmann, R., and L. Malagnini (2004). Interpretation of high frequency ground motion from regional seismic network observations, *Bull. Seism. Soc. Am.* (in press).
- Joyner, W., and D. Boore (1993). Methods for regression analysis of strong-motion data, *Bull. Seism. Soc. Am.* **83**, 469–487.
- Joyner, W. B., and D. M. Boore (1994). Errata, *Bull. Seism. Soc. Am.* **84**, 955–956.
- Kennett, B. (1986). Lg waves and structural boundaries, *Bull. Seism. Soc. Am.* **76**, 1133–1141.
- Lermo, J., and F. Chavez-Garcia (1993). Site effect evaluation using spectral ratios with only one station, *Bull. Seism. Soc. Am.* **83**, 1574–1594.
- Nakamura, Y. (1989). A method for dynamic characteristics estimation of subsurface using microtremor on the ground surface, *QR RTRI* **30**, 25–33.
- Ou, G., and R. Herrmann (1990). A statistical model for peak ground motion from local to regional distances, *Bull. Seism. Soc. Am.* **80**, 1397–1417.
- Seht, M., and J. Wohlenberg (1999). Microtremor measurements used to map thickness of soft sediments, *Bull. Seism. Soc. Am.* **89**, 250–259.
- Shin, T., and R. Herrmann (1987). Lg attenuation and source studies using 1982 Miramichi data, *Bull. Seism. Soc. Am.* **77**, 384–397.
- Siddiqi, J., and G. Atkinson (2002). Ground motion amplification at rock sites across Canada, as determined from the horizontal-to-vertical component ratio, *Bull. Seism. Soc. Am.* **92**, 877–884.
- Somerville, P., and J. Yoshimura (1990). The influence of critical Moho reflections on strong ground motions recorded in San Francisco and Oakland during the 1989 Loma Prieta earthquake, *Geophys. Res. Lett.* **17**, 1203–1206.
- Sonley, E. (2004). Investigation of earthquake attenuation in the Charlevoix, Quebec, seismic zone, *Ph.D. Thesis*, Carleton University, Ottawa, Canada.
- Theodulidis, N., P. Bard, R. Archuleta, and M. Bouchon (1996). Horizontal-to-vertical spectral ratio and geological conditions: the case of Garner Valley downhole array in southern California, *Bull. Seism. Soc. Am.* **86**, 306–319.
- Toro, G., N. Abrahamson, and J. Schneider (1997). Model of strong ground motions from earthquakes in central and eastern North America: best estimates and uncertainties, *Seism. Res. Lett.* **68**, 41–57.
- Tsuboi, S., M. Saito, and Y. Ishihara (2001). Verification of horizontal-to-vertical spectral-ratio technique for estimation of site response using borehole seismographs, *Bull. Seism. Soc. Am.* **91**, 499–510.

Carleton University  
Dept. Earth Sciences  
Ottawa, ON, K1S 5B6, Canada

Manuscript received 19 August 2003.